Thermal aspect of the diurnal variation of tropical convective and stratiform rainfall*

Cui Xiao-Peng(崔晓鹏)[a)†] and Li Xiao-Fan(李小凡)[b)]

[a)] *Laboratory of Cloud-Precipitation Physics and Severe Storms (LACS), Institute of Atmospheric Physics, Chinese Academy of Sciences, Beijing* 100029, *China*

[b)] *NOAA/NESDIS/Office of Research and Applications, Camp Springs, Maryland, USA*

(Received 20 December 2010; revised manuscript received 19 April 2011)

The diurnal variation of radiation plays a key role in determining the diurnal variations of tropical oceanic convective and stratiform rainfall, and the examination of such a relationship requires a direct link between the radiation term in a heat budget and the surface rain rate in a cloud budget. Thus, the thermally related surface rainfall budgets derived from the combination of cloud and heat budgets are analysed with two-dimensional equilibrium cloud-resolving model simulation data to study the effects of sea surface temperature (SST) and cloud radiative, and microphysical processes on the diurnal variations of convective and stratiform rainfall. The results show that the increase in SST, the inclusion of diurnal variation of SST and the exclusion of cloud radiative processes increase negative diurnal anomalies of heat divergence over rainfall-free regions during the nighttime through changing the vertical structures of diurnal anomaly of radiation in the troposphere. The strengthened negative diurnal anomalies of heat divergence over rainfall-free regions enhance positive diurnal anomalies of heat divergence over convective regions, which intensifies the positive diurnal anomaly of convective rainfall. The exclusion of microphysical effects of ice clouds increases the negative diurnal anomaly of heat divergence over rainfall-free regions during the nighttime through reducing latent heat; this appears to enhance the positive diurnal anomaly of heat divergence over raining stratiform regions, and thus stratiform rainfall.

Keywords: thermal aspects, diurnal variation, tropical convective and stratiform rainfall

PACS: 92.60.Ox, 92.40.Ea, 92.05Fg, 92.60.Nv **DOI:** 10.1088/1674-1056/20/10/109201

1. Introduction

As one of the most important meteorological cycles, the diurnal cycle of oceanic deep convective activity and associated rainfall has been intensively debated both observationally and numerically for over half a century.[1−10] Studies have concentrated on the relationship between radiative cooling and the nocturnal rainfall peak, the main component of diurnal rainfall variation.

Rainfall comes from convective and raining stratiform regions. Compared to stratiform rainfall, convective rainfall is associated with higher rain rates, stronger upward motion and horizontal reflectivity gradients. The accretion of cloud water by raindrops via collisions in strong updraft cores mainly accounts for convective rainfall, whereas the vapor deposition on ice particles is mainly responsible for the development of stratiform rainfall.[11] Nesbitt and Zipser[12] conducted an observational study and found that the magnitude of the diurnal cycle of convective rainfall is larger than that of stratiform rainfall. To study the effects of water vapor on rainfall, the surface rain rate in the cloud budget is directly linked to water vapor processes in the water vapor budget. Thus, Gao *et al.*[13] combined water vapor and cloud budgets to derive the water vapor-related surface rainfall budget. Water vapor-related surface rainfall budgets have been examined by Cui,[14] Gao and Li,[15] Cui and Li,[16] and Ping and Luo[17] to study the effects of sea surface temperature and cloud radiative and microphysical processes on the diurnal variations of convective and stratiform rainfall. Cui[14] carried out the diurnal analysis of the surface rainfall budget and found that a higher convective rain rate is associated with more vapor convergence, and a higher stratiform rain

*Project supported by the National Basic Research Program of China (Grant No. 2009CB421505), the Funds for International Cooperation and Exchange of the National Natural Science Foundation of China (Grant No. 40921160379), and the National Natural Science Foundation of China (Grant No. 40775036).

†Corresponding author. E-mail: xpcui@mail.iap.ac.cn

© 2011 Chinese Physical Society and IOP Publishing Ltd

rate is related to more vapor convergence and more local atmospheric drying in the early morning than in the afternoon. Cui and Li[16] studied the effects of diurnal variation of the imposed sea surface temperature (SST) on the diurnal variation of convective and stratiform rainfall, and revealed that a high SST in the afternoon transports a large amount of water vapor from rainfall-free regions to convective regions and increases afternoon rainfall. Ping and Luo[17] examined the microphysical and radiative effects of ice clouds on diurnal variations of tropical convective and stratiform rainfall and found that the exclusion of ice radiative effects generally increases convective rainfall during the morning and the evening, and reduces convective rainfall in the afternoon. However, the exclusion of ice microphysical effects generally reduces convective and stratiform rainfall during the morning and increases convective and stratiform rainfall in the afternoon and the evening.

The above studies revealed the important effects of water vapor processes on the diurnal variation of tropical rainfall, but they did not provide a clear physical picture of how nighttime radiative cooling determines the nocturnal rainfall peak, the key component of diurnal variation of tropical rainfall. The examination of such a relationship requires an equation that directly links the radiation term in a heat budget and the surface rain rate in a cloud budget. Recently, Gao and Li[18] derived a thermally related surface rainfall equation by combining heat and cloud budgets, and applied the equation to the analysis of the diurnal variation of tropical rainfall during the Tropical Ocean Global Atmosphere Coupled Ocean Atmosphere Response Experiment (TOGA COARE). The objective of the present study is to apply the thermally related surface rainfall budget to the analysis of rainfall data to reveal how SST and cloud radiative and microphysical processes influence diurnal variations of convective and stratiform rainfall by changing the diurnal variation of radiation. To achieve this, the thermally related surface rainfall budget will be analysed using data from two-dimensional (2D) equilibrium sensitivity cloud-resolving model simulations. The model and the experiments are briefly described in the next section. The results are presented in Section 3. A summary is given in Section 4.

2. Model and experiment

The simulation data analysed in this study are from Gao *et al.*,[19] Ping *et al.*,[20] and Gao and Zhou.[21] The cloud-resolving model used in these simulations is a 2D version of the model used by Sui *et al.*[7,22] and further modified by Li *et al.*[23]. The model was originally developed by Soong and Ogura,[24] Soong and Tao,[25] and Tao and Simpson.[26] The model has cyclic lateral boundaries and includes five prognostic equations for the mixing ratios of cloud water, raindrops, cloud ice, snow and graupel, and a prognostic equation for potential temperature, specific humidity and perturbation momentum. The model also includes cloud microphysical parameterization schemes[27−31] and solar and thermal infrared radiation parameterization schemes.[32−34] The model uses a horizontal domain of 768 km, a horizontal grid resolution of 1.5 km, 33 vertical levels and a time step of 12 s. The cloud-resolving model has been applied to the study of tropical convection.[14,16,18,35] A detailed model description can be found in Ref. [15] by Gao and Li.

All simulations from Gao *et al.*,[19] Ping *et al.*,[20] and Gao and Zhou[21] are integrated for 40 days with the 2D cloud-resolving model with a constant, uniform zonal wind and zero large-scale vertical velocity. The vertical profiles of temperature and specific humidity observed at 156° E and 1.75° S during TOGA COARE at 0400 LST 19 December 1992[6] are used as the initial conditions. The increase in SST leads to the increase in mass-weighted mean air temperature and precipitable water, whereas the diurnal variations of SST cause cooling.[19] The diurnal variation of the solar zenith angle produces atmospheric warming and moistening.[19,21] The exclusions of ice radiative and microphysical effects[20] and cloud radiative effects[21] generate atmospheric cooling and drying.

The model simulations are summarized in Table 1. SST29 and SST31 use the same model setup except that different time-invariant SSTs of 29 °C and 31 °C are used, respectively. These experiments are used to study the effects of SST on the diurnal variation of rainfall. SST29D has diurnally varied SSTs with a mean of 29 °C and a diurnal amplitude of 1 °C. The comparison of SST29D with SST29 shows the effects of the diurnal variation of SST on the diurnal variation of rainfall. Experiments SST29NIR and SST29NWR are identical to SST29 except that SST29NIR and SST29NWR exclude the

radiative effects of ice and water clouds, respectively, by setting the mixing ratio of ice and water hydrometeors to zero in the calculations of optical depth and radiation. The comparisons between SST29NCR and SST29, SST29NIR and SST29, SST29NWR and SST29, respectively, reveal cloud, ice and water radiative effects. Experiment SST29NIM excludes ice-cloud variables and associated ice microphysical and radiative processes by turning off the ice microphysics scheme during the model integration. The comparison between SST29NIM and SST29NIR shows the microphysical effects of ice clouds under the conditions of no ice radiative effects. The hourly instantaneous grid data from day 21 to day 40 are used to study the diurnal variations in the following discussion. The diurnal variations of convective and stratiform rain rates in the control experiment (SST29) and their sensitivities to the diurnal variation of SST (SST29D),[16] microphysical and radiative effects of ice clouds (SST29NIR and SST29NIM),[17] and cloud radiative effects (SST29NCR)[15] have been studied with the analysis of vapor-related surface rainfall budgets. The local time is used in the following discussion.

Table 1. Summary of experiments.

Experiment	SST	Solar zenith angle	Radiation	Ice microphysics
SST29	time-invariant (29 °C)	diurnally varied	yes	yes
SST31	time-invariant (31 °C)	diurnally varied	yes	yes
SST29D	diurnally varied with mean of 29 °C and maximum diurnal difference of 1 °C	diurnally varied	yes	yes
SST29NCR	time-invariant (29 °C)	diurnally varied	no for both water and ice clouds	yes
SST29NIR	time-invariant (29 °C)	diurnally varied	no for ice clouds	yes
SST29NWR	time-invariant (29 °C)	diurnally varied	no for water clouds	yes
SST29NIM	time-invariant (29 °C)	diurnally varied	no for ice clouds	no

To study the diurnal variation of rainfall, the diurnal anomaly of rainfall is calculated by removing the time-mean from the diurnal composite of the rainfall. The maximum positive diurnal anomaly of model domain mean rain rate in SST29 (0.055 mm·h^{-1}) occurs around hour 5 (not shown here). The maximum positive diurnal anomaly of the 150-km averaged rain rate in disturbed period of the TOGA COARE (0.13 mm·h^{-1}) appears around hour 3 [see Fig. 4(a) in Sui *et al.*[6]], whereas the maximum rain rate during the 21-day period of the COARE from 18 December 1992 to 9 January 1993 occurs at around hour 1 [see Fig. 5 in Ref. [36] by Gao *et al.* The observed nocturnal rainfall peaks may be affected by large-scale circulations and their timings may be different. However, maximum nocturnal rainfall peaks usually occur from midnight to hour 7 since it results primarily from infrared radiative cooling, which reduces the saturation specific humidity and makes condensation easier.[6,7,18] The model with temporally varying large-scale forcing from COARE simulates the maximum rainfall around hour 1 in the control experiment of Gao *et al.*[36] The model is capable of simulating the diurnal variations of tropical oceanic rainfall. Gao and Li[18] showed that the maximum positive diurnal anomaly of the model domain mean surface rain rate (0.18 mm·h^{-1}) is at around hour 5 in their experiment CR when the model is imposed with time-mean large-scale forcing during the 21-day COARE period from 18 December 1992 to 9 January 1993. The difference in the timing of the nocturnal rainfall peak between the simulations with time-invariant large-scale forcing and with time-dependent large-scale forcing may result from the diurnal variations of large-scale vertical velocity [see Fig. 2 in Ref. [36] by Gao *et al.* To focus on the effects of the diurnal variation of radiation on the diurnal variation of rainfall, the control experiment in SST29 and sensitivity experiments are conducted using a model imposed with zero large-scale vertical velocity.

The maximum positive diurnal anomaly of 150-km averaged rain rate in an undisturbed period of TOGA COARE (0.02 mm·h^{-1}) appears around hours 13–18 while the negative diurnal anomaly of rain rate occurs during the nighttime (see Fig. 12 in Ref. [6] by Sui *et al.*). The nocturnal rainfall during an

undisturbed period may be suppressed by large-scale subsidence. The model imposed with zero large-scale vertical velocity in SST29D produces a higher model domain mean surface rain rate than in SST29 from hour 16 to midnight (0.02 mm·h^{-1}–0.05 mm·h^{-1} for SST29D-SST29) while both experiments produce large nocturnal rainfall (see Fig. 2 in Ref. [16] by Cui and Li). The diurnal variation of SST imposed in SST29D has a maximum around hour 16, which lags the maximum solar zenith angle by 4 hours (not shown) because the ocean surface is continuously heated by solar radiation after the solar zenith angle has reached its maximum.

To study these effects on the diurnal variations of convective and stratiform rainfall, the convective-stratiform cloud partitioning method is employed. The method was originally developed by Tao *et al.*[37,38] and modified by Sui *et al.*[22] In this study, each vertical column containing clouds is partitioned into convective or stratiform based on the following criteria. Model grid points in the surface rain field, which have a rain rate twice as large as the average taken over the surrounding four grid points are taken as the cores of convective cells. For each core grid point, the grid point on either side is also considered convective. In addition, any grid point with a rain rate of 20 mm·h^{-1} or more is designated as being convective regardless of the above criteria. All nonconvective cloudy points are regarded as being stratiform. Grid points in the stratiform regions are further checked and classified as being convective if (i) in the precipitating stratiform regions, cloud water below the melting level is greater than 0.5 g·kg^{-1} or the maximum updraft above 600 hPa exceeds 5 m·s^{-1}, or (ii) in the nonprecipitating stratiform regions, cloud water exists (cloud water is greater than 0.025 g·kg^{-1}) or the maximum updraft exceeds 5 m·s^{-1} below the melting level.

Precipitation is intimately associated with both water vapor and heat processes. Thus, combinations of cloud budget with water vapor and heat budgets through the net condensation term lead to vapor-related and thermally related surface rainfall budgets, respectively. Following Gao *et al.*[13] and Cui and Li,[39] the vapor-related surface rainfall budget can be written as

$$P_s = Q_{\rm WVT} + Q_{\rm WVF} + Q_{\rm WVE} + Q_{\rm CM}, \quad (1)$$

$$Q_{\rm WVT} = -\frac{\partial\,[q_{\rm v}]}{\partial t}, \quad (1a)$$

$$Q_{\rm WVF} = -\Big[\bar{u}^{\rm o}\frac{\partial \bar{q}_{\rm v}}{\partial x}\Big] - \Big[\frac{\partial(u'q'_{\rm v})}{\partial x}\Big] - \Big[\bar{u}^{\rm o}\frac{\partial q'_{\rm v}}{\partial x}\Big] - \Big[w'\frac{\partial \bar{q}_{\rm v}}{\partial z}\Big], \quad (1b)$$

$$Q_{\rm WVE} = E_{\rm s}, \quad (1c)$$

$$Q_{\rm CM} = -\frac{\partial\,[q_5]}{\partial t} - \Big[u\frac{\partial q_5}{\partial x}\Big] - \Big[w\frac{\partial q_5}{\partial z}\Big]. \quad (1d)$$

Following Li[40] and Gao and Li,[18] the thermally-related surface rainfall equation can be expressed as

$$P_{\rm S} = S_{\rm HT} + S_{\rm HF} + S_{\rm HS} + S_{\rm LHLF} + S_{\rm RAD} + Q_{\rm CM}, \quad (2)$$

where

$$S_{\rm HT} = \frac{c_{\rm p}}{L_{\rm v}}\frac{\partial\,[T]}{\partial t}, \quad (2a)$$

$$S_{\rm HF} = \frac{c_{\rm p}}{L_{\rm v}}\Big[\frac{\partial}{\partial x}(\bar{u}^{\rm o}+u')T' + \pi\bar{u}^{\rm o}\frac{\partial\,\bar{\theta}^{\rm o}}{\partial x} + \pi\bar{w}^{\rm o}\frac{\partial}{\partial z}(\bar{\theta}+\theta') + \pi w'\frac{\partial\bar{\theta}}{\partial z}\Big], \quad (2b)$$

$$S_{\rm HS} = -\frac{c_{\rm p}}{L_{\rm v}}H_{\rm s}, \quad (2c)$$

$$S_{\rm LHLF} = -\frac{L_{\rm f}}{L_{\rm v}}\langle P_{18}\rangle, \quad (2d)$$

$$S_{\rm RAD} = -\frac{1}{L_{\rm v}}\langle Q_R\rangle. \quad (2e)$$

$$\begin{aligned} P_{18} = {} & P_{\rm DEP} + P_{\rm SDEP} + P_{\rm GDEP} - P_{\rm MLTS} - P_{\rm MLTG} \\ & + P_{\rm SACW}(T<T_{\rm o}) + P_{\rm SFW}(T<T_{\rm o}) \\ & + P_{\rm GACW}(T<T_{\rm o}) + P_{\rm IACR}(T<T_{\rm o}) \\ & + P_{\rm GACR}(T<T_{\rm o}) + P_{\rm SACR}(T<T_{\rm o}) \\ & + P_{\rm GFR}(T<T_{\rm o}) - P_{\rm RACS}(T>T_{\rm o}) \\ & - P_{\rm SMLT}(T>T_{\rm o}) - P_{\rm GMLT}(T>T_{\rm o}) \\ & + P_{\rm IHOM}(T<T_{\rm oo}) - P_{\rm IMLT}(T>T_{\rm o}) \\ & + P_{\rm IDW}(T_{\rm oo}<T<T_{\rm o}). \end{aligned} \quad (2f)$$

In Eqs. (1) and (2), u and w are zonal and vertical components of wind, respectively; total hydrometeor mixing ratio $q_5 = q_{\rm c} + q_{\rm r} + q_{\rm i} + q_{\rm s} + q_{\rm g}$, $q_{\rm c}, q_{\rm r}, q_{\rm i}, q_{\rm s}, q_{\rm g}$ are the mixing ratios of cloud water, raindrop, cloud ice, snow and graupel, respectively; $\overline{u}^{\rm o} = 4$ m·s^{-1}; T and θ are air temperature and potential temperature, respectively; $\pi = (p/p_0)^{\kappa}$, $\kappa = R/c_{\rm p}$, R is the gas constant, $c_{\rm p}$ is the specific heat of dry air at constant pressure; $H_{\rm s}$ is the surface sensible heat flux; $L_{\rm v}$, $L_{\rm s}$, and $L_{\rm f}$ are latent heats of vaporization, sublimation and fusion at $T_{\rm o} = 0$ °C, respectively, $L_{\rm s} = L_{\rm v} + L_{\rm f}$,; $T_{\rm oo} = -35$ °C; cloud microphysical processes in Eq. (2f) can be found in Table 2; $Q_{\rm R}$ is the radiative heating rate due to the convergence of net flux

of solar and infrared radiative fluxes; overbar denotes a model domain-mean; a prime refers to a perturbation from the model domain mean; the symbol ° is an imposed forcing; mass integration $[(\ )] = \int_{z_b}^{z_t} \overline{\rho}(\ )\mathrm{d}z$, and z_t and z_b are the heights of the top and bottom of the model atmosphere, respectively. The vapor-related surface rainfall budget (1) states that the surface rain rate (P_S) is determined by local atmospheric moistening ($Q_{WVT} < 0$)/drying ($Q_{WVT} > 0$), water vapor convergence ($Q_{WVF} > 0$)/divergence ($Q_{WVF} < 0$), surface evaporation (Q_{WVE}), and decrease of local hydrometeor concentration/hydrometeor convergence ($Q_{CM} > 0$) or increase of local hydrometeor concentration/hydrometeor divergence ($Q_{CM} < 0$). The thermally related surface rainfall budget (2) states that the surface rain rate (P_S) is determined by local atmospheric cooling ($S_{HT} < 0$)/warming ($S_{HT} > 0$), heat divergence ($S_{HF} > 0$)/convergence ($S_{HF} < 0$), surface sensible heat (S_{HS}), latent heat due to ice-related processes (S_{LHLF}), radiative cooling ($S_{RAD} > 0$)/heating ($S_{RAD} < 0$) and a decrease of local hydrometeor concentration/hydrometeor convergence ($Q_{CM} > 0$) or an increase of local hydrometeor concentration/hydrometeor divergence ($Q_{CM} < 0$).

Table 2. List of microphysical processes and parameterization schemes from Rutledge and Hobbs 1983 (RH83),[28] 1984 (RH84);[29] Lin *et al.* 1983 (LFO),[27] Tao *et al.* 1989 (TSM),[30] and Krueger *et al.* 1995 (KFLC).[31]

Notation	Description	Scheme
P_{MLTG}	growth of vapor by evaporation of liquid from graupel surface	RH84
P_{MLTS}	growth of vapor by evaporation of melting snow	RH83
P_{REVP}	growth of vapor by evaporation of raindrops	RH83
P_{IMLT}	growth of cloud water by melting of cloud ice	RH83
P_{CND}	growth of cloud water by condensation of supersaturated vapor	TSM
P_{GMLT}	growth of raindrops by melting of graupel	RH84
P_{SMLT}	growth of raindrops by melting of snow	RH83
P_{RACI}	growth of raindrops by the accretion of cloud ice	RH84
P_{RACW}	growth of raindrops by the collection of cloud water	RH83
P_{RACS}	growth of raindrops by the accretion of snow	RH84
P_{RAUT}	growth of raindrops by the autoconversion of cloud water	LFO
P_{IDW}	growth of cloud ice by the deposition of cloud water	KFLC
P_{IACR}	growth of cloud ice by the accretion of rain	RH84
P_{IHOM}	growth of cloud ice by the homogeneous freezing of cloud water	
P_{DEP}	growth of cloud ice by the deposition of supersaturated vapor	TSM
P_{SAUT}	growth of snow by the conversion of cloud ice	RH83
P_{SACI}	growth of snow by the collection of cloud ice	RH83
P_{SACW}	growth of snow by the accretion of cloud water	RH83
P_{SFW}	growth of snow by the deposition of cloud water	KFLC
P_{SFI}	Depositional growth of snow from cloud ice	KFLC
P_{SACR}	growth of snow by the accretion of raindrops	LFO
P_{SDEP}	growth of snow by the deposition of vapor	RH83
P_{GACI}	growth of graupel by the collection of cloud ice	RH84
P_{GACR}	growth of graupel by the accretion of raindrops	RH84
P_{GACS}	growth of graupel by the accretion of snow	RH84
P_{GACW}	growth of graupel by the accretion of cloud water	RH84
P_{WACS}	growth of graupel by the riming of snow	RH84
P_{GDEP}	growth of graupel by the deposition of vapor	RH84
P_{GFR}	growth of graupel by the freezing of raindrops	LFO

3. Results

The diurnal anomalies of convective and stratiform rain rates and associated thermally related surface rainfall budgets over convective, raining stratiform and rainfall-free (non-raining stratiform plus clear sky) regions are averaged in the 12-hour nighttime (hours 1–6 and 19–24) in all experiments (Table 3). The corresponding diurnal anomalies of rainfall and budgets averaged over the daytime (hours 7–18) are not shown because they simply have the opposite signs to the diurnal anomalies of rainfall and

budgets averaged over the nighttime. Thus, only the diurnal anomaly of rainfall and its processes will be analysed in the following discussion. Cui[14] analysed the vapor-related surface rainfall budget in SST29 and showed that more water vapor convergence yields a higher convective rain rate and that more vapor convergence and more local vapor loss cause higher stratiform rain rate in early morning than in the afternoon. The positive diurnal anomaly of convective rain rate in SST29 is nearly twice as large as that of the stratiform rain rate (Table 3). The positive diurnal anomaly of the convective rain rate is primarily associated with the positive diurnal anomaly of heat divergence ($S_{\rm HF}$) over convective regions, whereas the positive diurnal anomaly of the stratiform rain rate is mainly related to the positive diurnal anomalies of radiation ($S_{\rm RAD}$) and heat divergence over raining stratiform regions. The positive diurnal anomaly of heat divergence over convective regions is mainly balanced by the negative diurnal anomaly of heat divergence over rainfall-free regions, which is in turn offset by the positive diurnal anomaly of radiation.

Table 3. Diurnal anomalies of surface rain rate ($P_{\rm S}$), local heat change ($S_{\rm HT}$), heat convergence ($S_{\rm HF}$), radiative heating ($S_{\rm RAD}$), and hydrometeor convergence minus storage ($Q_{\rm CM}$) over (a) convective regions, (b) raining stratiform regions, and (c) rainfall-free regions averaged in the nighttime (hours 1–6 and 19–24) in SST29, SST31, SST29D, SST29NIR, SST29NIM, SST29NCR, and SST29NWR. $S_{\rm HS}$ and $S_{\rm LHLF}$ are not shown due to negligibly small diurnal anomalies. Unit is mm·h^{-1}.

(a)	SST29	SST31	SST29D	SST29NIR	SST29NIM	SST29NCR	SST29NWR
$P_{\rm S}$	0.0130	0.0258	0.0176	0.0210	0.0216	0.0220	0.0213
$S_{\rm HT}$	−0.0006	0.0002	−0.0034	−0.0006	−0.0018	−0.0001	−0.0008
$S_{\rm HF}$	0.0148	0.0277	0.0227	0.0315	0.0262	0.0318	0.0208
$S_{\rm RAD}$	0.0041	0.0047	0.0042	0.0045	0.0040	0.0048	0.0036
$Q_{\rm CM}$	−0.0053	−0.0065	−0.0058	−0.0141	−0.0067	−0.0140	−0.0022

(b)	SST29	SST31	SST29D	SST29NIR	SST29NIM	SST29NCR	SST29NWR
$P_{\rm S}$	0.0072	0.0118	0.0085	0.0064	0.0103	0.0077	0.0065
$S_{\rm HT}$	−0.0005	−0.0011	−0.0010	−0.0022	0.0004	−0.0013	−0.0012
$S_{\rm HF}$	0.0025	0.0043	0.0027	−0.0053	0.0067	−0.0050	0.0019
$S_{\rm RAD}$	0.0045	0.0045	0.0045	0.0039	0.0017	0.0035	0.0050
$Q_{\rm CM}$	0.0007	0.0041	0.0022	0.0097	0.0015	0.0099	0.0008

(c)	SST29	SST31	SST29D	SST29NIR	SST29NIM	SST29NCR	SST29NWR
$S_{\rm HT}$	−0.0751	−0.0610	−0.0721	−0.0637	−0.0608	−0.0648	−0.0703
$S_{\rm HF}$	−0.0173	−0.0320	−0.0254	−0.0263	−0.0329	−0.0268	−0.0227
$S_{\rm RAD}$	0.0935	0.0930	0.0946	0.0894	0.0894	0.0904	0.0927
$Q_{\rm CM}$	−0.0007	0.0003	0.0023	0.0006	0.0043	0.0012	0.0007

The positive diurnal anomaly of the convective rain rate in SST31 is about twice as large as that in SST29 because the positive diurnal anomaly of heat divergence over the convective regions in SST31 is nearly twice as large as that in SST29 (Table 3(a)). The positive diurnal anomaly of the stratiform rain rate in SST31 is also larger than that in SST29, due mainly to the increase in the positive diurnal anomalies of $Q_{\rm CM}$ and $S_{\rm HF}$ (Table 3(b)). Compared with the case of SST29, the larger positive diurnal anomaly of heat divergence over convective regions in SST31 is balanced mainly by the larger negative diurnal anomaly of heat divergence over rainfall-free regions. While the positive diurnal anomalies of radiation in the two experiments are similar, the larger negative diurnal anomaly of heat divergence leads to the smaller negative diurnal anomaly of local heat change ($S_{\rm HT}$) in SST31 than in SST29. Although the two experiments have similar positive diurnal anomalies of radiation, they have different vertical structures of radiation, as indicated by Fig. 1(a). The response of diurnal anomaly of heat divergence to the diurnal anomaly of radiation is limited below 15 km due to negligibly weak vertical motion above 15 km. While the mass integration of diurnal anomaly of radiation is about zero, the large negative difference in diurnal anomaly of heat divergence between SST31 and SST29 below 10 km and the small positive difference above 10 km yield negative difference in diurnal anomaly of heat divergence between SST31 and SST29.

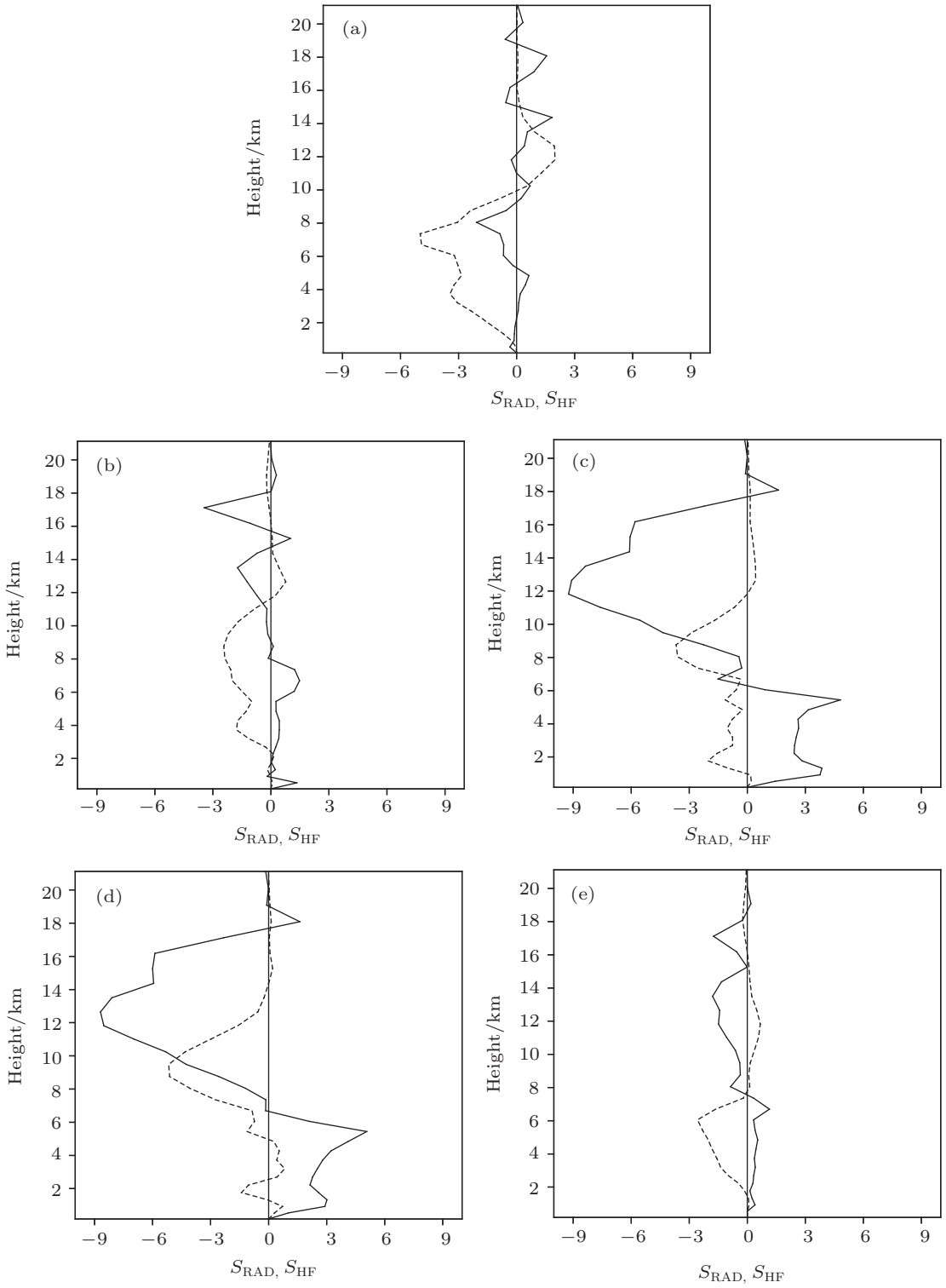


Fig. 1. Diurnal anomalies of vertical profiles of radiation (S_{RAD}) (solid lines) and heat divergence (S_{HF}) (dash lines) averaged over the nighttime (hours 1–6 and 19–24) in the rainfall-free regions for (a) SST31–SST29, (b) SST29D–SST29, (c) SST29NIR–SST29, (d) SST29NCR–SST29, and (e) SST29NWR–SST29. Unit is 10^{-3} h^{-1}.

Cui and Li[16] conducted a comparison study of vapor-related surface rainfall budgets and cloud microphysical budgets over convective regions between SST29 and SST29D and showed that in the late afternoon, a larger amount of water vapor is pumped into rainfall-free region through the larger surface evaporation associated with the warmer SST. More water vapor is then transported into convective regions to produce more vapor condensation and more collection of cloud water by raindrops and larger convec-

tive rainfall in SST29D than in SST29. The inclusion of diurnal variation of SST in SST29D increases positive diurnal anomalies of convective and stratiform rain rates, respectively, by 35.4% and 18.1% (Table 3). The increase of positive diurnal anomaly of convective rainfall is associated primarily with the increase in positive diurnal anomaly of heat divergence over convective regions, whereas the increase of positive diurnal anomaly of stratiform rainfall is related mainly with the increase in positive anomaly of $Q_{\rm CM}$. The increase in positive diurnal anomaly of heat divergence over convective regions is nearly balanced by the increase in negative diurnal anomaly of heat divergence over rainfall-free regions. The dominant negative difference in diurnal anomaly of heat divergence between SST29D and SST29 corresponds to the positive difference in diurnal anomaly of radiation below 8 km, which is nearly offset by the negative differences above 8 km in mass integration (Fig. 1(b)).

Ping and Luo[17] examined the radiative and microphysical effects of ice clouds on vapor-related surface rainfall budgets and revealed that the difference in the diurnal anomaly of convective rainfall is associated primarily with the difference in the diurnal anomaly of water vapor convergence over convective regions. The analysis of thermally related surface rainfall budgets in the two experiments here shows that the exclusion of radiative effects of ice clouds in SST29NIR increases positive diurnal anomaly of convective rain rate by 61.5% and decreases positive diurnal anomaly of stratiform rain rate by 11.1% (Table 3). The increase of positive diurnal anomaly of convective rainfall corresponds to the increase in positive diurnal anomaly of heat divergence over convective regions, whereas the decrease of positive diurnal anomaly of stratiform rainfall is related primarily to the change in heat divergence from the positive diurnal anomaly in SST29 to the negative diurnal anomaly in SST29NIR. The exclusion of radiative effects directly influences vertical structure of difference in radiation between SST29NIR and SST29 over rainfall-free regions. The IR cooling is stronger below 6 km in SST29NIR than in SST29 (Fig. 1(c)) because the exclusion of radiative effects of ice clouds in SST29NIR enhances more IR cooling than in SST29 by allowing more IR radiation to space. The difference in the diurnal anomaly of heat divergence between SST29NIR and SST29 over rainfall-free regions generally becomes negative, which corresponds to the diurnal anomaly of radiation. The increase in the negative diurnal anomaly of heat divergence over rainfall-free regions leads to the increase in the positive diurnal anomaly of heat divergence over convective regions, and thus the increase in the positive diurnal anomaly of convective rainfall in SST29NIR.

The positive diurnal anomaly of convective rainfall is insensitive to microphysical effects of ice clouds because the decrease in the positive diurnal anomaly of heat divergence by the exclusion of microphysical effects of ice clouds over convective regions in SST29NIM is nearly balanced by the decrease in the negative diurnal anomaly of $Q_{\rm CM}$ (Table 3). In contrast, the exclusion of microphysical effects of ice clouds increase the positive diurnal anomaly of stratiform rain rate by 60.9%, due primarily to the change in heat divergence over raining stratiform regions from the negative diurnal anomaly in SST29NIR to the positive diurnal anomaly in SST29NIM, which is in turn associated with the increase in negative diurnal anomaly of heat divergence over rainfall-free regions. The exclusion of microphysical effects of ice clouds in SST29NIM directly removes ice-related latent heat and deposition processes from the model. Thus, the latent heat that is approximated by the sum of $S_{\rm HT}$, $S_{\rm HF}$, and $S_{\rm RAD}$ in heat budget is calculated. The diurnal anomalies of latent heat are -0.0043 mm$\cdot$h^{-1} in SST29NIM and -0.0006 mm$\cdot$h^{-1} in SST29NIR. The exclusion of microphysical effects of ice clouds in SST29NIM causes the larger negative diurnal anomaly of latent heat over rainfall-free regions in SST29NIM than in SST29NIR, which is responsible for the increase in the positive diurnal anomaly of stratiform rainfall.

Gao and Li[15] found the positive difference in convective rainfall and similar stratiform rainfall between SST29 and SST29NCR (see their Figs. 8.8 and 8.9). The comparison of vapor-related surface rainfall budgets between SST29 and SST29NCR reveals that the positive difference in convective rainfall is associated primarily with the positive difference in water vapor convergence over convective regions, which is balanced mainly by the negative difference in water vapor convergence in raining stratiform regions. The negative difference in water vapor convergence in raining stratiform regions is balanced by the positive difference, i.e. local water vapor storage and hydrometeor convergence minus storage, which leads to a similar stratiform rainfall. In this study, the increment of the positive diurnal anomaly of convective rain rate by the exclusion of cloud radiative effects

(both ice and water radiative effects) in SST29NCR and by the exclusion of radiative effects of water clouds in SST29NWR is similar to the increment of the positive diurnal anomaly of convective rain rate by the exclusion of radiative effects of ice clouds in SST29NIR, while the positive diurnal anomalies of stratiform rain rate are less sensitive to cloud, water, and ice radiative effects (Table 3). Over rainfall-free regions, the similar vertical structures of difference in diurnal anomalies of radiation between SST29NCR and SST29 (Fig. 1(d)) and between SST29NIR and SST29 (Fig. 1(c)) produce similar vertical structures of negative difference in the diurnal anomalies of heat divergence, whereas the negative difference in the diurnal anomaly of heat divergence between SST29NWR and SST29 corresponds to the positive difference in the diurnal anomaly of radiation between the mid and lower troposphere (Fig. 1(e)). The increases in the negative diurnal anomaly of heat divergence over rainfall-free regions for SST29NCR, SST29NIR and SST29NWR lead to the increase in positive diurnal anomaly of heat divergence, and thus the increase of positive diurnal anomaly of convective rainfall.

4. Summary

Diurnal variations of convective and stratiform rainfalls are intimately associated with the diurnal variations of water vapor and heat processes. The effects of sea surface temperature and cloud radiative and microphysical processes on the diurnal variations of water vapor processes have been intensively investigated with the analysis of water vapor-related surface rainfall budgets in the previous studies.[14−17] However, the diurnal variation of radiation, an important part in thermal balance, plays a key role in determining the diurnal variation of surface rainfall.[7,18,36] The examination of this key thermal relationship with surface rainfall requires a direct link between the radiation term in the heat budget and the surface rain rate in the cloud budget. Thus, the two budgets were combined by Gao and Li[18] to form the thermally related surface rainfall budget. In this study, thermally related surface rainfall budget is applied to the analysis of equilibrium sensitivity cloud-resolving model simulation data to study the effects of sea surface temperature and cloud radiative and microphysical processes on the diurnal variations of convective and straitiform rainfall. The analysis of thermally related surface rainfall budgets shows that although the SST and cloud radiative and microphysical processes have little influence on the diurnal anomaly of the mass-integrated radiation term, they significantly affect the vertical structures of the diurnal anomaly of radiation. The responses of the vertical structures of the diurnal anomaly of heat divergence and their mass-integrations to radiation are regulated by the vertical structure of the vertical velocity and are sensitive to the effects of sea surface temperatureand cloud radiative and microphysical processes, which leads to the sensitivity of surface rainfall to these effects.

The analysis of these sensitivity experiments is conducted by taking the averages of diurnal anomalies of convective and stratiform rain rates and associated thermal processes in the 12 hours of the nighttime (local hours 1–6 and 19–24). The increase in SST, the inclusion of diurnal variation of SST and the exclusion of the radiative effects of water clouds and ice clouds increase the positive diurnal anomaly of convective rain rate during the nighttime, mainly through increasing the positive diurnal anomaly of heat divergence over convective regions. The increases in positive diurnal anomaly of heat divergence over convective regions are nearly balanced by the increases in negative diurnal anomaly of heat divergence over rainfall-free regions, which correspond to the change in diurnal anomaly of radiation in the troposphere. In contrast, these effects have a less important effect on the diurnal anomaly of stratiform rain rate. The exclusion of microphysical effects of ice clouds removes ice-related latent heat over rainfall-free regions (in particular, over non-raining stratiform regions) and so enhances the negative diurnal anomaly of heat divergence there and the positive diurnal anomaly of heat divergence over raining stratiform regions, and thus increases the positive diurnal anomaly of stratiform rainfall. The diurnal anomaly of convective rainfall is insensitive to the microphysical effects of ice clouds.

Note that these experiments are conducted with an imposed zero large-scale vertical velocity in a 2D model and are highly idealized in comparison to observations in which non-zero large-scale forcing usually interact with convective systems.[6] Gao *et al.*[36] conducted the cloud-resolving model simulations that are imposed by large-scale forcing during the selected periods of TOGA COARE and zero large-scale vertical velocity, separately, to study the diurnal variation of tropical rainfall and found that the diurnal variations of radiation in the simulation with imposed zero vertical velocity is responsible for the nocturnal rain-

fall peak but non-zero large-scale forcing may affect the diurnal amplitudes of rainfall. The interaction between large-scale forcing and convective systems may affect the diurnal amplitudes of tropical rainfall in the sensitivity experiments.

While 2D and three-dimensional (3D) model simulations are similar in the aspects of collective thermodynamic feedback effect, vertical transport of mass, sensible heat and moisture, thermodynamic field, surface heat flux, surface precipitation, precipitation efficiency, and convective and moist vorticity vectors,[41−49] their comparison reveals differences. Tompkins[50] showed that 2D model simulations produce stronger convective cold pools than those produced by 3D model simulations. Petch[51] found that the use of a 2D model has the largest effect on the development of convection. Stephens *et al.*[52] revealed the differences in precipitable-water and precipitation variability and upper-tropospheric cloud fraction and condensate amount between 2D and 3D model simulations. Therefore, the effects of sea surface temperature and cloud radiative and microphysical processes on diurnal variation of rainfall and associated processes needs further study by using a 3D cloud-resolving model imposed by a non-zero large-scale vertical velocity.

References

[1] Kraus E B 1963 *J. Atmos. Sci.* **20** 546

[2] Gray W M and Jacobson R W 1977 *Mon. Wea. Rev.* **105** 1171

[3] Randall D A, Harshvardhan D and Dazlich A 1991 *J. Atmos. Sci.* **48** 40

[4] Sui C H and Lau K M 1992 *Mon. Wea. Rev.* **120** 407

[5] Tao W K, Lang S, Simpson J, Sui C H, Ferrier B and Chou M D 1996 *J. Atmos. Sci.* **53** 2624

[6] Sui C H, Lau K M, Takayabu Y N and Short D 1997 *J. Atmos. Sci.* **54** 639

[7] Sui C H, Li X and Lau K M 1998 *J. Atmos. Sci.* **55** 2345

[8] Liu C and Moncrieff M W 1998 *J. Atmos. Sci.* **55** 2329

[9] Yang S, Kuo K S and Smith E A 2008 *J. Climate* **21** 4115

[10] Ping F and Luo Z 2009 *Acta Phys. Sin.* **58** 4319 (in Chinese)

[11] Houghton H G 1968 *J. Appl. Meteor.* **7** 851

[12] Nesbitt S W and Zipser E J 2003 *J. Climate* **16** 1456

[13] Gao S, Cui X, Zhou Y and Li X 2005 *J. Geophys. Res.* **110** D10202 doi:10.1029/2004JD005467

[14] Cui X 2008 *J. Geophys. Res.* **113** D02113 doi: 10.1029/2007JD008990

[15] Gao S and Li X 2008 *Cloud-resolving Modeling of Convective Processes* (Berlin: Springer) p. 206

[16] Cui X and Li X 2009 *Meteor. Atmos. Phys.* **104** 53

[17] Ping F and Luo Z 2009 *Atmos. Res.* **93** 862

[18] Gao S and Li X 2010 *J. Geophys. Res.* **115** doi: 2009JD0012452

[19] Gao S, Zhou Y and Li X 2007 *J. Atmos. Sci.* **64** 656

[20] Ping F, Luo Z and Li X 2007 *Mon. Wea. Rev.* **135** 2794

[21] Gao S and Zhou Y 2008 *Geophys. Res. Lett.* **35** L15815 doi: 10.1029/2008GL034340

[22] Sui C H, Lau K M, Tao W K and Simpson J 1994 *J. Atmos. Sci.* **51** 711

[23] Li X, Sui C H, Lau K M and Chou M D 1999 *J. Atmos. Sci.* **56** 3028

[24] Soong S T and Ogura Y 1980 *J. Atmos. Sci.* **37** 2035

[25] Soong S T and Tao W K 1980 *J. Atmos. Sci.* **37** 2016

[26] Tao W K and Simpson J 1993 *Terr. Atmos. Oceanic Sci.* **4** 35

[27] Lin Y L, Farley R D and Orville H D 1983 *J. Climate Appl. Meteor.* **22** 1065

[28] Rutledge S A and Hobbs P V 1983 *J. Atmos. Sci.* **40** 1185

[29] Rutledge S A and Hobbs P V 1984 *J. Atmos. Sci.* **41** 2949

[30] Tao W K, Simpson J and McCumber M 1989 *Mon. Wea. Rev.* **117** 231

[31] Krueger S K, Fu Q, Liou K N and Chin H N S 1995 *J. Appl. Meteor.* **34** 281

[32] Chou M D, Kratz D P and Ridgway W 1991 *J. Climate* **4** 424

[33] Chou M D, Suarez M J, Ho C H, Yan M M H and Lee K T 1998 *J. Climate* **11** 202

[34] Chou M D and Suarez M J 1994 *NASA Tech. Memo.* 104606, Vol. 3, p. 85 available from NASA/Goddard Space Flight Center, Code 913, Greenbelt, MD 20771

[35] Cui X 2008 *Chin. Phys.* B **17** 2304

[36] Gao S, Cui X and Li X 2009 *Adv. Atmos. Sci.* **26** 895

[37] Tao W K, Simpson J, Lang S, McCumber M, Adler R and Penc R 1990 *J. Appl. Meteor.* **29** 1232

[38] Tao W K, Simpson J and Soong S T 1991 *Mon. Wea. Rev.* **119** 2699

[39] Cui X and Li X 2006 *J. Geophys. Res.* **111** D17112 doi:10.1029/2005JD006876

[40] Li X 2009 *J. Tropical Meteor.* **15** 148

[41] Tao W K and Soong S T 1986 *J. Atmos. Sci.* **43** 2653

[42] Tao W K, Simpson J and Soong S T 1987 *J. Atmos. Sci.* **44** 3175

[43] Grabowski W W, Wu X, Moncrieff M W and Hall W D 1998 *J. Atmos. Sci.* **55** 3264

[44] Khairoutdinov M F and Randall D A 2003 *J. Atmos. Sci.* 60 607

[45] Gao S, Ping F, Li X and Tao W K 2004 *J. Geophys. Res.* **109** D14106 doi:10.1029/2004JD004807

[46] Gao S, Cui X, Zhou Y, Li X and Tao W K 2005 *J. Geophys. Res.* **110** D17104 doi: 10.1029/2004JD005675

[47] Gao S, Li X, Tao W K, Shie C L and Lang S 2007 *J. Geophys. Res.* **112** D01105 doi: 10.1029/2006JD007179

[48] Sui C H, Li X, Yang M J and Huang H L 2005 *J. Atmos. Sci.* **62** 4358

[49] Zeng X, Tao W K, Zhang M, Peters-Lidard C, Lang S, Simpson J, Kumar S, Xie S, Eastman J L, Shie C L and Geiger J V 2007 *J. Atmos. Sci.* **64** 4153

[50] Tompkins A M 2000 *Mon. Wea. Rev.* **128** 1521

[51] Petch J C 2006 *Quart. J. Roy. Meteor. Soc.* **132** 345

[52] Stephens G L, van den Heever S and Pakula L 2008 *J. Atmos. Sci.* **65** 3899